Time-domain waveform processing by chromatic dispersion for temporal shaping of optical pulses

Robert E. Saperstein, Nikola Alić, Dmitriy Panasenko, Rostislav Rokitski, and Yeshaiahu Fainman

Department of Electrical and Computer Engineering, University of California, San Diego, 9500 Gilman Drive, La Jolla, California 92093-0409

Received December 16, 2004; revised manuscript received May 17, 2005; accepted May 18, 2005

We describe a novel method for subpicosecond pulse shaping based on longitudinal spectral decomposition in dispersive media. The entire system is created with standard telecommunications equipment allowing for integration with optical communication networks. The technique has the potential for time–bandwidth products $\geqslant 10^4$ due to exclusive reliance on time-domain processing. We introduce the principle of operation and subsequently support it with results from our experimental system. Both theory and experiments suggest third-order dispersion as the principle limitation to realizing a large number of resolvable spots. Chirped fiber Bragg gratings offer a route to increase the time–bandwidth product for high-speed signal processing applications.

OCIS codes: 320.5540, 070.6020, 260.2030.

1. INTRODUCTION

A number of science and engineering applications, including coherent quantum control and optical communications, motivate research in optical pulse shaping.[1,2] Fourier synthesis methods are broadly implemented to achieve desired shaped pulsed waveforms with subpicosecond temporal features. In such an approach the produced optical signal is composed of a waveform proportional to the input pulse convolved with the Fourier transform (FT) of an applied spectral filter. When exploiting the space domain to perform signal processing, liquid-crystal and acousto-optic (AO) modulators provide the means for introduction of somewhat arbitrary system transfer functions.[3,4] Traditionally, a pair of gratings and lenses is used to decompose and compose the spectral content of the pulsed, optical waveforms.[5] More recently, compact waveguide-based approaches have used arrayed waveguide gratings (AWGs) to perform an analogous spectral decomposition to those achieved with traditional free-space coupled gratings.[6]

Pulse-shaping arrangements with the space domain for transverse spectral decomposition offer excellent phase manipulation for applications that perform quantum control. These approaches have limitations, however, when one is creating waveforms for optical communications. Coupling shaped waveforms back into a single-mode fiber (SMF) introduces loss and limits the temporal extent of generated pulse shapes. The origin of this restraint is the time–space interrelation inherent in traditional pulse-shaping devices.[7] Spatial–temporal pulse shapers used with diffraction gratings and lenses have a spatial offset between advanced and delayed pulses in the transverse mode of the output optical waveform. A subsequent launch into the output fiber windows the spatial mode and thus also windows the created pulse shape in time. AWG approaches rely on the complex waveguide elements to circumvent this problem, but they are also practically limited by fabrication requirements. The number of resolvable spots in the output waveform for both Fourier synthesis and direct space-to-time AWG approaches[6,8] is equal to the number of waveguide channels. An alternative approach to pulse shaping that relyies on a single transverse spatial mode can better integrate with fiber systems and ultimately has the potential for large achievable time–bandwidth products (TBWPs).

Our research concentrates on creating a fiber-integrated, subpicosecond pulse-shaping technique utilizing standard optical communications equipment. A Fourier synthesis approach succeeds in the time domain when we use chromatic dispersion for longitudinal spectral decomposition. A time variant element (e.g., modulator) filters this spectral decomposition wave (SDW). Conjugating the dispersion-based optical system through propagation in a dispersive source matched (i.e., of opposite sign but equal magnitude) to the first dispersive element recomposes the pulsed waveform. Thus the number of resolvable spots relies on a suitable modulation scheme and the experimental ability to stretch and recompress a subpicosecond pulse using second-order dispersion. The fiber-based approach offers a route to in-line pulse-shaping operation spanning long propagation distances, while the potential for large TBWPs is appealing to high-speed signal processing applications.

In a recent publication we proposed and demonstrated the application of the novel pulse-shaping technique for the performance of microwave spectrum analysis.[9] The work centers on the modulation of a spectrally decomposed subpicosecond pulse in time with an arbitrary microwave signal. At the output additional satellite pulses appear in the optical waveform corresponding to the spectral sidebands of the modulating signal. Spectral decomposition is performed using dispersive propagation in op-

tical fiber. Descriptions focus on validating the approach for microwave spectrum analysis. However, a treatment of the technique as a generalized pulse-shaping approach was omitted. In this work, we seek to clarify the nature of the generalized temporal processing approach to pulse shaping with regard to idealizations and practicalities of dispersion and electro-optic (EO) modulation. We show that chromatic dispersion provides a viable means for generation of SDWs of subpicosecond pulses with application for pulse shaping. We also describe and demonstrate the distortions associated with higher-order chromatic dispersion considering both the degrading and the beneficial effects.

Section 2 contains analysis of the generalized dispersion-based pulse-shaping technique. The nature of output pulses from such a system is explored and contrasted with the optical waveforms produced in traditional spatial–temporal pulse-shaping schemes. An experimental demonstration and results are shown in Section 3 and discussions are included in Section 4. Section 5 concludes the paper.

2. ANALYSIS

A dispersive medium generates a temporal SDW from a launched transform-limited pulse through a variation in group velocities across the optical bandwidth. Drawing on the identical mathematical treatments of diffraction in space and dispersion in time,[10] an approximate FT of an incident optical signal is achieved by chromatic dispersion after reaching the so-called far-field approximation. With such an amount of dispersion, the temporal waveform closely resembles the spectrum.[11] Varying the propagation distance or the strength of the second-order dispersion parameter affects linearly the time duration of the SDW. Decreasing the temporal duration of the launched transform-limited pulse will also increase the time duration of the SDW as this waveform must support the entire bandwidth of the optical pulse. Over the past decade researchers have experimentally altered dispersion-induced SDWs to perform pulse shaping. The writing of a spectral filter into a chirped fiber Bragg grating (CFBG) has been used to both generate and spectrally shape such a dispersed waveform.[12,13] The inability to reconfigure this type of grating with present technologies is a chief drawback. To circumvent this problem, an EO modulator driven by an arbitrary waveform can follow the source of chromatic dispersion to alter the dispersed temporal waveform[1] and perform time-domain spectral shaping.[14] However, while the spectral intensity of such an optical signal may be shaped, the possibility to directly create temporal features shorter than ~10 ps in the dispersed optical signal is impossible due to limits on modulation speeds. It has been suggested,[14] and in this work we demonstrate and explain, that use of a conjugate dispersive element of equal magnitude but opposite sign can recompose the shaped optical waveform to a first approximation.

A general description of our novel pulse-shaping technique, shown in Fig. 1, includes propagation through a dispersive element, an EO modulator, and a conjugate dispersive element. Analogous to the transfer function of

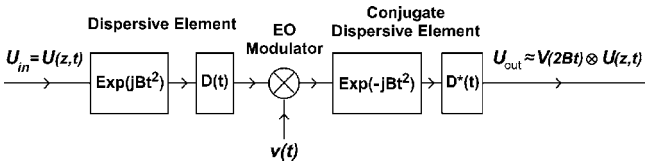

Fig. 1. Block diagram description of the pulse-shaping technique based on standard electrical system schematics. U_{in} and U_{out} are the input and output pulse envelopes, respectively. $U(z,t)$ is the launched pulse envelope, $\nu(t)$ is the modulating signal, and $V(2Bt)$ is the microwave signal spectrum scaled to time. The boxes contain impulse responses associated with passage through the respective element. In the boxes associated with second-order dispersion, $B=1/(2\beta_2 z)$, while in the others $D(t)$ and $D^*(t)$ represent the impulse responses originating from all higher-order dispersion terms.

free space, dispersive propagation is treated as contributing a quadratic spectral phase. Thus in Fig. 1 a quadratic phase impulse response is included for both dispersive elements. For completeness the propagation constant $\beta(\omega)$ is expanded in a Taylor series around the carrier frequency ω_c, and all terms with coefficients above β_2 (where $\beta_2 = \partial^2\beta/\partial\omega^2|_{\omega_c}$) are lumped into a distortion term. The resulting spectral phases are Fourier transformed to give the distortion impulse responses, $D(t)$ and $D^*(t)$, in the block diagram. By applying $\nu(t)$ to the modulator, the electrical signal, by the EO effect and the Mach–Zehnder structure of the modulator, spectrally filters the optical SDW in time. The conjugate dispersive element recomposes the optical signal and gives an output waveform with pulses $U(z,t)$ at temporal shifts corresponding to all spectral components of $\nu(t)$. The pulses generated from the ac components of $\nu(t)$ are referred to here as satellite pulses, but they can be thought of as sidebands. A central pulse, corresponding to an unmodulated optical signal, relates to the dc component of $\nu(t)$. In pulse-shaping applications, $\nu(t)$ is chosen to achieve general optical waveforms.

To first order our pulse-shaping technique has advantageous properties when we are determining the maximum number of resolvable spots contained in generated optical waveforms. Because of the linearity of the system, temporal resolution is locked to the transform-limited duration of the input pulse. However, long and detailed pulse shapes can be generated by creating fine spectral features. If the size of the point-spread function in the SDW is much smaller than the features of the filter, spectral feature size can be decreased in two ways. The size of a single element in the spectral filter can be decreased or, alternatively, the dimension of the SDW can be increased. In these directions spatial–temporal techniques are limited commonly by a finite spatial entrance pupil, grating resolution, and/or finite feature sizes in the spectral filters. The desire to increase the number of resolvable spots requires that these traditional pulse-shaping techniques grow in spatial dimension to achieve a large, high-resolution SDW. The demands, incurred through expansion in spatial dimensions, on the complexity of the optical components eventually prove a hindrance to further improvement. In contrast to spatial processing techniques, the time aperture created by the SDW of an optical pulse in dispersive media grows longer simply with

continued propagation. Furthermore, when increasing spectral resolution in this manner, the requirements on the spectral filter also prove advantageous. An EO modulator used to filter this SDW is immune to an increase in temporal dimension. In contrast, with a spatial processing approach (in the high-resolution limit of the SDW) a spatial light modulator employed as a spectral filter must grow in transverse dimension to match an increased aperture. With the ability to create long duration SDWs and utilize high-speed modulators for spectral filtering, the dispersion-based pulse-shaping technique has the potential for unprecedented TBWPs.

A theoretical description of the pulse-shaping technique begins in the frequency domain to facilitate inclusion of higher-order dispersion terms using transfer functions. An analogous time-domain description, not including distortions, can be found in Ref. 9. Although all terms from the expansion of $\beta(\omega)$ will have an effect on the dispersion-based pulse-shaping technique, experimentally β_2 and β_3 (the second and third orders) prove most important. The former provides the linear separation of spectral components necessary for SDW generation while the latter acts as the strongest system distortion (i.e., aberration). Our analysis and implementation center on use of optical fibers as the source of chromatic dispersion due to widespread availability. CFBGs are also considered theoretically for their controllable dispersion characteristics. Optical nonlinearities can be discounted in dispersion-compensated links for subpicosecond pulses provided that optical powers are maintained at levels that do not lead to self-phase modulation (SPM).[15] SPM, if present, would degrade the ability to recompress the optical pulse. However, the nonlinear regime is beyond the scope of this paper, and experimental measures were taken to assure a linear regime of operation. All passive elements in the system are treated as linear and time invariant. Moreover, as we make use of the slowly varying envelope approximation, our analysis is valid only for launched pulses greater than $\sim$100 fs.[16]

Consider a subpicosecond transform-limited pulse at $z=0$ with its spectrum $U(0,\omega)$ propagating along the z axis. Here ω represents a shifted spectrum around the carrier frequency, i.e., $\omega=\Omega-\omega_c$ if Ω is absolute frequency. The optical field at the output of the first dispersive element, assumed to provide anomalous dispersion ($\beta_2<0$), is represented through the multiplication of the spectrum of the pulse at $z=0$ with a quadratic phase and cubic phase, yielding

$$U(z,\omega)=U(0,\omega)\exp\left(-j\frac{1}{2}\beta_2 z\omega^2\right)\exp\left(-j\frac{1}{6}\beta_3 z\omega^3\right). \quad (1)$$

As $|\beta_2|\gg|\beta_3|$ for materials and spectral operating points of interest, the quadratic phase is the dominant dispersive effect. The strength of this phase term depends on the value of β_2 and on z, the propagation length. In the time domain the pulse propagates to the far field when the condition $|\beta_2 z|\gg\tau^2/2$, where τ is the transform-limited pulse half-width, is satisfied. This regime is mathematically equivalent to transitioning from Fresnel to Fraunhofer diffraction, and it signifies that the quadratic phase term across the temporal aperture of the launch pulse in the Fresnel integral is approximately unity. Thus the relationship $|\beta_2 z|\gg\tau^2/2$ indicates the propagation requirements needed to achieve a SDW in the time domain. With a dispersion in a SMF of $\beta_2=-20$ ps^2/km and pulses of $\sim$0.1 ps duration, the far field is achieved within only a few meters of fiber.

Modulating the dispersed waveform with ideal signal ν(t) and then propagating through a dispersion-compensating element providing standard dispersion lead to an output waveform in the frequency domain:

$$U_{\text{out}}(z,\omega)=\left\{\int_{-\infty}^{\infty}V(\omega-\omega')U(0,\omega')\times\exp\left[-j\frac{1}{2}\beta_2 z(\omega')^2-j\frac{1}{6}\beta_3 z(\omega')^3\right]\mathrm{d}\omega'\right\}\times\exp\left(-j\frac{1}{2}\beta_2' z'\omega^2-j\frac{1}{6}\beta_3' z'\omega^3\right). \quad (2)$$

Here we used the fact that multiplication of the SDW in the time domain by $\nu(t)$ corresponds to convolution in the frequency domain between $V(\omega)$ and the SDW of Eq. (1). When making the Fraunhofer approximation, the filtering signal $\nu(t)$ can be expressed as modulating the spectrum of the optical pulse directly, analogous to the operation of spatial light modulators in traditional spatial–temporal pulse shapers. However, for accuracy in our model, modulation is restricted to the time domain, and the spectrum of $\nu(t)$ is convolved with the spectrum of the chirped pulse.

Matching dispersive elements for complete compensation of second- and third-order dispersion is possible but necessitates extreme care. When only second-order dispersion is considered, we must strive to balance all propagation lengths to precise tolerances. A trial-and-error approach varying the lengths of the two media can succeed to exactly match the magnitudes of $\beta_2 z$ and $\beta'_2 z'$. However, when third-order dispersion is considered, we rely on the dispersive device manufacturers to appropriately create the dispersion and dispersion slope of each element. If $\beta_3 z$ is to simultaneously match $\beta'_3 z'$ when second-order dispersion is compensated, the ratio of β_2 to β'_2 must exactly equal the ratio of β_3 to β'_3. Optical fiber manufacturers developed dispersion-compensating fibers (DCFs) that are matched to their SMF products, prompting an initial assumption that complete dispersion compensation of both β_2 and β_3 is fair. Presuming the two dispersive elements are exactly matched, the second dispersive element contributes quadratic and cubic phases identical to those of the first but opposite in their signs. Therefore $\beta'_2 z'$ and $\beta'_3 z'$ are equal to $\beta_2 z$ and $\beta_3 z$ in magnitude, respectively. For simplicity of notation both quadratic phase terms will have strength $\beta_2 z$ while the first, carried from Eq. (1), will be set positive (i.e., β_2 is negative) to represent propagation in the anomalous dispersion regime. The second, entering in Eq. (2), will remain negative for standard dispersion. For the cubic phase terms, $\beta'_3 z'$ is set equal to negative $\beta_3 z$ following the case in commercial SMFs and DCFs.

Examining a sample modulation signal helps to understand the physical meaning of Eq. (2). If the modulator

provides a microwave signal with dc and components at fundamental frequency, ω_0, then $V(\Omega)=A\delta(\Omega)+B\delta(\Omega-\omega_0)+B\delta(\Omega+\omega_0)$. Note that we assume the period $2\pi/\omega_0$ to be shorter than the time aperture created by the SDW. Inserting the signal $V(\omega)$ into Eq. (2), performing the convolution, expanding the exponentials, and multiplying the dispersion compensation phase terms leads to

$$\begin{aligned} U_{\text{out}}(z,\omega) = AU(z,\omega) + \Bigg\{ & BU(z,\omega-\omega_0) \\ & \times \exp\left[j\frac{1}{6}(3\beta_2 z + \beta_3 z\omega_0)\omega_0{}^2 \right] \\ & \times \exp\left[-j\left(\beta_2 z + \frac{1}{2}\beta_3 z\omega_0 \right)\omega_0\omega \right] \\ & \times \exp\left(j\frac{1}{2}\beta_3 z\omega_0\omega^2 \right) \Bigg\} + \Bigg\{ BU(z,\omega+\omega_0) \\ & \times \exp\left[j\frac{1}{6}(3\beta_2 z - \beta_3 z\omega_0)\omega_0{}^2 \right] \times \exp\left[j\left(\beta_2 z \right.\right. \\ & \left.\left. - \frac{1}{2}\beta_3 z\omega_0 \right)\omega_0\omega \right] \exp\left(-j\frac{1}{2}\beta_3 z\omega_0\omega^2 \right) \Bigg\}. \end{aligned} \tag{3}$$

The three copies of the original pulse spectrum correspond to the frequency makeup of the modulating signal $\nu(t)$, i.e., the dc signal and sidebands, respectively. The linear phase affecting the two frequency-shifted pulses signifies the temporal advancement and delay of these satellite pulses. However, we observe that the original transform-limited pulse waveform is obtained only for the first copy of the pulse spectrum in Eq. (3), whereas a quadratic phase modulates the other two. This quadratic spectral phase will chirp and broaden the satellite pulses in the same way chromatic dispersion operates, and, most importantly, its strength is proportional to the frequency of modulation. Performing an inverse FT on Eq. (3) provides a time-domain output for the system. The operation is simplified by transforming the pulse, constant phase and linear phase together, independently from the quadratic spectral phase. In the time domain, the transforms are rejoined by a convolution integral represented by the operator $\otimes$ as follows:

$$\begin{aligned} U_{\text{out}}(z,t) = {} & AU(z,t)\exp(j\omega_c t) \\ & + \Bigg\{ B\exp\left[-j\left(\frac{1}{2}\beta_2 z + \frac{1}{3}\beta_3 z\omega_0 \right)\omega_0{}^2 \right] \\ & \times \exp[j(\omega_c+\omega_0)t] \times U\left(z, t - \beta_2 z\omega_0 - \frac{1}{2}\beta_3 z\omega_0{}^2 \right) \\ & \otimes \exp\left(-j\frac{t^2}{2\beta_3 z\omega_0} \right) \Bigg\} + \Bigg\{ B\exp\left[-j\left(\frac{1}{2}\beta_2 z \right.\right. \\ & \left.\left. - \frac{1}{3}\beta_3 z\omega_0 \right)\omega_0{}^2 \right] \exp[j(\omega_c-\omega_0)t] \times U\left(z, t + \beta_2 z\omega_0 \right. \\ & \left. - \frac{1}{2}\beta_3 z\omega_0{}^2 \right) \otimes \exp\left(j\frac{t^2}{2\beta_3 z\omega_0} \right) \Bigg\}. \end{aligned} \tag{4}$$

The first term, representing the dc signal, is both transform limited and free of a temporal shift. The two satellite pulses, representing the sidebands, are shifted temporally from the central position on the time axis. The temporal shifts of $\pm\beta_2 z\omega_0$ are the desired result of the pulse-shaping procedure. However, the presence of third-order dispersion provides a secondary temporal shift that, although small, must be considered for signal processing. More detrimental is the convolution of the satellite pulses with a quadratic phase, which leads to temporal broadening and a respective decrease in their peak power. Because the amount of temporal broadening is directly proportional to the microwave carrier frequency ω_0, satellite pulses temporally shifted farther from the central pulse will see larger temporal expansion. Ultimately, large temporal shifts will lead to a lack of temporal confinement and peak power that may prove inadequate for pulse-shaping applications and detection systems. This physical result has a space-domain analog. It is known that spatially filtering the spatially dispersed spectrum of a signal in free space leads to chirped satellite pulses.

As an aide for potential users, a figure of merit for the system is defined as the temporal shift, T_D, of a satellite pulse that results in a doubling of pulse duration. If the pulses are assumed Gaussian, the quadratic phase resulting from β_3 broadens the satellite pulses as $T_1=T_0[1+(\beta_3 z\omega_0/T_0^2)^2]^{1/2}$, where T_0 and T_1 are the transform-limited and broadened half-widths at a $1/e$ intensity point.[16] The temporal shift of each satellite pulse is $T_S=\beta_2 z\omega_0$, if the small shift due to β_3 is ignored. Thus we determine that when $T_1/T_0=2$, $T_S=T_D=\sqrt{3}T_0^2\beta_2/\beta_3$. For a system employing commercial communication fiber with $\beta_2\approx-20$ ps^2/km and $\beta_3\approx0.1$ ps^3/km and a laser source producing pulses with $T_0\approx0.1$ ps, T_D is roughly 4 ps. It should be noted that if β_3 is reduced relative to β_2, the broadening of satellite pulses becomes less severe as is reflected in the equation for T_D. Third-order dispersion then introduces a trade-off between design simplicity (use of commercial off-the-shelf fibers) and the performance (limited number of resolvable spots and TBWPs).

Although for some applications, shaped waveforms of limited temporal duration ($\sim$10 ps) may not be a problem, high-speed signal processing applications demand an alternative approach, which realizes larger TBWPs. Use of elements with tailored dispersion can result in a system without higher-order dispersion terms. Meter-long fiber Bragg gratings can be continuously written with controlled dispersion coefficients.[17] Thus, as an example, a CFBG could be employed in the fiber-integrated system to set β_3 and higher-order terms to zero. For such a system a FT of Eq. (3) is written as

$$\begin{aligned} U_{\text{out}}(z,t) = {} & AU(0,t)\exp(j\omega_c t) + \beta\exp\left(-j\frac{1}{2}\beta_2 z\omega_0{}^2 \right)U(0,t \\ & - \beta_2 z\omega_0)\exp[j(\omega_c+\omega_0)t] \\ & + B\exp\left(-j\frac{1}{2}\beta_2 z\omega_0{}^2 \right)U(0,t+\beta_2 z\omega_0) \\ & \times\exp[j(\omega_c-\omega_0)t]. \end{aligned} \tag{5}$$

Here the temporal shifts of the satellite pulses are propor-

tional to the strength of β_2 only, and the quadratic phase that broadens the satellite pulses is gone. Again the constant phase in Eq. (5) modulating the two sidebands is present but can be ignored. Because of far-field propagation, it results in negligible phase offsets between overlapping satellite pulses. A linear phase term modulating each satellite pulse in Eq. (5) remains from Eq. (4) and cannot be dismissed. These linear phases are seen to upshift and downshift the temporal bandwidth of the delayed and advanced pulses, respectively, by the modulation frequency. With use of an EO modulator for signal filtration, these Doppler shifts may approach tens of gigahertz. Although frequency shifts from the carrier are present in the satellite pulses created in traditional pulse-shaping methods as well, such shifts are smaller because slower modulators are utilized. To reduce the frequency shifts of the satellite pulses in our technique, a larger dispersion-induced time aperture is needed. As seen in Eqs. (4) and (5), temporal shifts of the satellite pulses are proportional to $\beta_2 z \omega_0$. Thus, for a given time shift, ω_0 can be decreased if z is increased. The coupling of time and frequency is a characteristic feature of the dispersive pulse-shaping system due largely to the nature of the approximate FT performed by propagation in a dispersive medium. Although the Doppler shift is removed under the far-field approximation [where all phase terms in Eq. (5) are set to one], it truly becomes insignificant only with extremely large time apertures and slow modulations speeds. Although not critical to all pulse-shaping applications, this dependence of frequency shifts on temporal shifts needs to be considered when one is performing signal processing.

The intensity waveform resulting from a simulation that follows the model developed by Eq. (5) is shown in Fig. 2(a). The modulating signal is identical to the $\nu(t)$ used in Eq. (3) where the coefficients are such that the dc component is stronger than the microwave signal ($A > B$). The launched 150 fs pulse was stretched to and compressed from a nanosecond with purely second-order dispersion, and the modulating tone is set such that ω_0 is equal to 14π Grad/s. Satellite pulses should appear at temporal locations $t = \pm \beta_2 z \omega_0$, which correspond to roughly ±2.3 ps as $\beta_2 z = 52$ ps^2. As a validation of the concept, it is apparent that the ratio of the temporal shift of the side pulses to the temporal width of the launched and recompressed pulse roughly equates with the ratio of the time window created by the dispersed pulse to the period of the modulating signal. Because of the difficulties in measuring optical waveforms with subpicosecond features, Fig. 2(b) shows the results of a practical solution to detection: an intensity autocorrelation (with background) of the signal in Fig. 2(a). For microwave spectrum analysis applications as described in Ref. 9, one can determine the microwave spectral content of an unknown signal $\nu(t)$ by examining the temporal waveform output from the system while scaling time to frequency by $t/\beta_2 z = \omega$. Equation (5) provides an identical result to the time-domain analysis performed in Ref. 9 if $\nu(t)$ from this example is inserted into Eq. of Ref. 9 and the convolution is carried out there. For general pulse-shaping applications, desired pulse shapes are created through the control of the modulating signal $\nu(t)$.

In a complete description of the pulse-shaping process, the details of the modulation scheme must be considered. Expected results rest heavily on one understanding the nature of how the SDW is modulated. It is apparent that the SDW creates a time aperture over which the modulation signal is windowed. For a spectral component of $\nu(t)$ to create a satellite pulse distinguishable from the dc pulse at the system output, its period must be shorter than the time aperture. A stretched SDW time aperture also cannot be permitted to extend into the SDW from the following or preceding pulse in the train. Thus the repetition rate of the laser system places an upper limit on dispersive propagation length and time aperture duration and a lower limit on the speed of $\nu(t)$. Regarding the maximization of temporal shifts for satellite pulse (e.g., TB-WPs or number of resolvable spots), higher-order dispersion introduces the most stringent confinement. When this effect is removed or disregarded, as in Eq. (5), modulator speed becomes the principle limit. The largest temporal shifts ($T_S = \beta_2 z \omega_0$) occur when both the speed of the modulator (ω_0) and the duration of the SDW time aperture ($\sim \beta_2 z$) are maximized. Of additional importance to

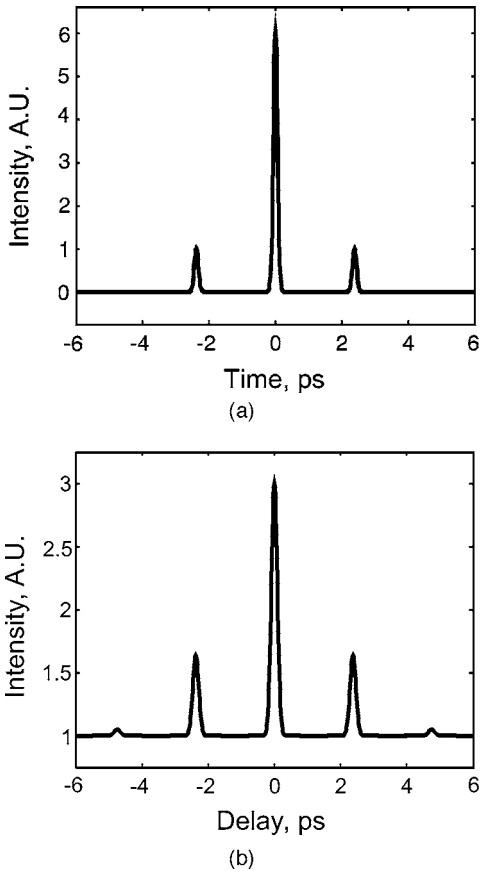

Fig. 2. (a) Intensity of a temporal waveform output from the system modeled by Eq. (4). Time is measured relative to the central pulse corresponding to the constant (dc) component of the modulating signal $\nu(t)$. The satellite pulses relate to the microwave sidebands, ±7 GHz. Here the microwave signal is weaker than the dc. (b) Intensity autocorrelation trace (with background) of the optical waveform in (a). The small pulses occurring at ±4.7 ps are cross correlations of the pulses at ±2.3 ps in (a). The cross correlation of the dc spike and satellite pulses in (a) form the pulses at ±2.3 ps in (b).

SDW modulation is the nature of the EO modulator itself. The spectrum of the modulation applied to the dispersed optical field, represented in Eq. (2) as $V(\omega)$, depends not only on the applied microwave–radio-frequency (RF) signal, but also on the characteristics of this modulator. Mach–Zehnder devices commonly used for intensity modulation in optical communications are well understood, and a mathematical treatment is reserved for Appendix A. An important detail is that the pulse-shaping technique utilizes field modulation and not intensity modulation. Null biasing a standard communications modulator allows for linear application of a desired microwave signal to the optical field provided that the applied voltages do not approach a large fraction of V_π for the modulator. Under these conditions the bias and signal amplitudes applied to the EO modulator control the coefficients A and B in Eqs. (4) and (5).

3. EXPERIMENTAL SYSTEM AND RESULTS

The experimental approach to realize pulse shaping is shown schematically in Fig. 3. A Coherent Mira pumped optical parametric oscillator delivers 150 fs transform-limited pulses at 76 MHz and a nanojoule of energy per pulse. The matched dispersive elements are spools of SMF and a DCF module. The operating wavelength is tuned to 1.55 μm to minimize attenuation and realize substantial dispersion. A grating stretcher and attenuator precede coupling into the SMF to avoid optical nonlinear effects associated with the highest peak intensities. Approximately 2.6 km of SMF are employed to disperse the pulse to a nanosecond FWHM. That the dispersed and launched pulses have identical spectra, when the former is scaled to remove attenuation, confirms the dominance of dispersion over SPM in the SMF. Specifically for our launch conditions, the ratio of the dispersion length to the nonlinear length, sometimes denoted as the soliton number, equals $N^2 \approx 0.035$.[16] Dispersion compensation occurs in a DCF module providing −44 ps/nm. In the linear propagation regime the order of the two fiber types is arbitrary. However, it is worth noting that power levels necessary to induce SPM are higher in DCFs than in SMFs. Therefore, for operation close to the nonlinear threshold (i.e., where $N^2 > 0.1$), the system should proceed with DCF. Operation with pulse energies above a nanojoule is possible using significant prestretching and poststretching to lower peak powers below SPM inducing levels. Experimentally, launching pulses of the order of 100 fs requires that all fibers and prechirping devices be matched with high precision. The length of the SMF must be tailored to within a few meters of the ideal length to measure a subpicosecond pulse at the output. Spectral filtering by modulation is performed by a 10 Gbit/s $LiNbO_3$ Mach–Zehnder intensity modulator. The swept frequency source used to drive the modulator with single sinusoidal waveforms delivers electrical powers less than 24 dBm. An erbium-doped fiber amplifier (EDFA) follows the modulator to boost signal strength. Note that the erbium fiber provides standard dispersion and must be factored in when we are determining the amount of SMF required. The output waveform from the DCF is measured using a Michelson interferometer-based autocorrelator. To view the interferometric autocorrelation trace (ACT), an amplified silicon photodiode is operated in a nonlinear detection mode by two-photon absorption (TPA). The TPA detection scheme provides useful phase sensitivity that gives experimental verification of full pulse recompression after propagation in the DCF. The nonlinear detection also facilitates detection of the time- and frequency-shifted satellite pulses since the cross correlation of these pulses (within the autocorrelation of the entire waveform) will average to the background level with a slow linear detector. The intensity requirements of the TPA process, however, require that the EDFA be used in the system. If the

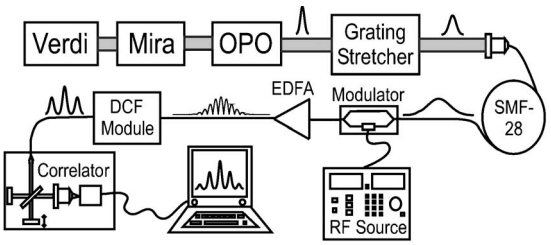

Fig. 3. Experimental setup for realization of subpicosecond pulse shaping. OPO, optical parametric oscillator.

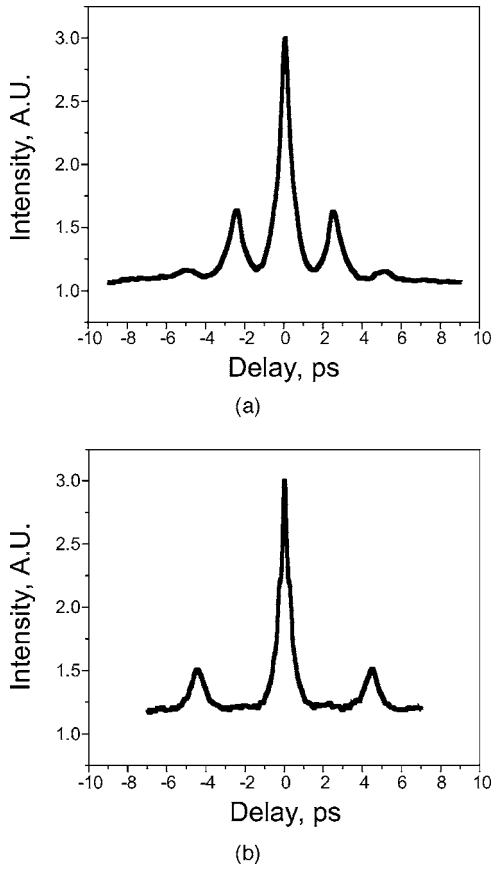

Fig. 4. Experimental intensity ACTs of signals with 7 GHz modulation. RF power is maintained at 15 dBm while the bias voltage is varied. (a) ACT in the presence of a strong dc component in the modulating signal $v(t)$. Experimental result shows agreement with the trace obtained from our linear model in Fig. 2(b). (b) ACT when the modulator was null biased. The autocorrelation process leads to the formation of three pulses as the inner two satellite pulses drop out.

system were not driving a nonlinear process, the EDFA could be omitted.

Detected results from the experimental setup described above are given in Fig. 4. The two intensity autocorrelations are generated through digital postprocessing of measured interferometric ACTs. In both cases the RF signal generator supplied a 7 GHz sinusoid with 15 dBm electrical power. In the experiments represented in Fig. 4(a) the bias to the modulator is controlled such that a strong dc (unmodulated) component is allowed to pass. Relating to Eqs. (4) and (5), the optical field can be described with coefficient A greater than coefficient B. The temporal shift, $t = \pm\beta_2 z\omega_0$, should correspond to ±2.3 ps. Correspondingly Fig. 4(a) shows close similarity to the modeling output of Fig. 2(b). Here again the small pulses at ±4.7 ps in the ACT are formed by the cross correlation of satellite pulses at ±2.3 ps in the output optical waveform. The strong central pulse in the output field cross correlating with a satellite pulse leads to the pulses at ±2.3 ps in the ACT. In Fig. 4(b) the modulator is null biased to completely remove the unmodulated component. The output field is described by setting A to zero in Eq. (4). Confirmation of carrier suppression is given by the complete removal of visible pulses at ±2.3 ps in the detected intensity ACT.

As stated, the choice of optical fiber as the low-loss dispersion element in our experimental setup stems from its widespread availability. However, a number of factors limit the ability of optical fiber to provide a true SDW. Both optical nonlinearities and higher-order dispersion terms can contribute to the degradation of the signal in a fiber-based implementation of the temporal pulse shaper. Although combating nonlinear effects is possible if high peak powers are avoided, the third-order dispersion of silica fiber must be considered. Thus, in practice, the complexities and drawbacks expressed in Eq. (4), as opposed to the simple description of Eq. (5), need to be used to describe the pulse-shaping system.

The experimental results confirming the presence of the temporal broadening with increased modulation frequency ω_0 as predicted in Eq. (4) are shown in Fig. 5. The EO modulator was again null biased to minimize the unmodulated component passing the modulator. The optical field following the dispersion compensation module contained two recompressed pulses, representing the upshifted and downshifted components. With three pulses in each overlaid ACT in Fig. 5, the advanced and delayed correlation pulses represent the cross correlation of the two pulses constituting the optical field. Visually comparing the FWHM of the advanced and delayed pulses corresponding to the 6 GHz modulation with those corresponding to the 3 GHz modulation clearly shows the broadening described theoretically.

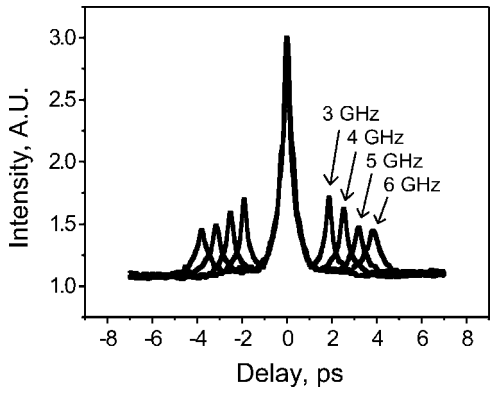

Fig. 5. Overlaid experimental intensity autocorrelations showing the effect of increased modulation frequency on a pulse-shaped waveform. The temporal broadening of the 6 GHz upshifted and downshifted pulses is apparent when comparing its FWHM with that of the 3 GHz side pulses.

4. DISCUSSION

Examining the experimental results in Fig. 5 leads to a better understanding of the roles of β_2 and β_3 and the importance of their proper compensation. The results shown in Fig. 5 depart somewhat from those predicted for an autocorrelation of the field expressed in Eq. (4) (where $A \ll B$). Each of the normalized curves in the overlaid intensity correlation traces is clearly not formed by a sequence of two equal pulses. Such a field, when correlated, should always form a central pulse of twice the height and similar width to the outer pulses in the trace. Furthermore, despite the increase in pulse duration with larger temporal shifts for the side pulses in Fig. 5, the central pulse remains markedly constant in width. The pulse triplets in the overlain ACTs of Fig. 5 must arise from optical signals containing two pulses of different peak intensities and durations. To better understand these optical fields that gave rise to the ACTs in Fig. 5, it is useful to reexamine the theoretical description of the distorted system described by Eqs. (3) and (4). The equations show that, whereas the length of the SMF and DCF can be set to produce only one transform-limited pulse at the output, this pulse need not be the central dc pulse. Adding the effect of residual second-order dispersion at the output of the DCF with the quadratic phase generated for upshifted and downshifted pulses due to β_3, a delayed or advanced pulse can be made to be nearly transform limited. In a system with exact β_3 cancellation, a small amount of second-order dispersion added to the field spectrum in Eq. (3) can cancel the term $\exp(\pm j1/2\beta_3 z\omega_0\omega^2)$ for a single satellite pulse. As an example, the residual quadratic phase given for an extra half-meter of SMF is nearly identical in magnitude to the quadratic phase resulting from β_3 for a 5 GHz shifted pulse in the experimental system described above. In such a case the advanced pulse in the output waveform is transform limited, while the delayed copy is twice as broad as it would be with exact β_2 cancellation. In general, using additional second-order dispersion to cancel the quadratic phase from β_3 leads to an advanced and delayed satellite pulse pair with a differential in amplitude and spreading that relates to the strength of β_3 and their distance from the central dc point. A small additional cubic phase is inevitable and would need to be practically considered. However, the idea lends itself to envisioning a system employing an adjustable dispersive element following the DCF designed to permit the user to select a satellite pulse from the output waveform to compensate and make it transform limited. Examples of such dispersive devices are a free-space grating stretcher or, as a more complex alternative, a traditional free-space pulse

shaper. For a microwave spectrum analysis technique, an operator could sweep across a spectral zone of interest maximizing the resolution at each point of observation, whereas for pulse shaping, the interplay of second- and third-order dispersion lends itself to the creation of asymmetric waveforms.

A confirmation of the theoretical description and experimental results is given in Fig. 6. The model used to produce the results of Figs. 2 and 4(a) is expanded to include the cubic spectral phases originating in a SMF and DCF. To negate additional pulse features, the cubic phases were set to balance precisely while the quadratic phases included a mismatch corresponding to 60 additional centimeters of SMF. Figure 6(a) shows the optical intensity after the DCF where the asymmetry of the pulsed waveforms is clearly visible for all frequencies of modulation. The temporally advanced pulse in all four cases is shown to be much closer to a transform-limited state than the delayed pulse. A set of overlaid intensity autocorrelations of the fields from Fig. 6(a) comprise Fig. 6(b). The result shows good agreement with the detected shape and microwave frequency dependence of Fig. 5. Because of the symmetry of the ACT, the intensity waveforms of Fig. 6(a) are not a unique solution to Fig. 6(b). A system lacking 60 cm of DCF would show an imbalance similar to Fig. 6(a) but with the temporally delayed pulse compressed relative to the leading pulse. The resulting ACTs would be identical. As such, we rely on our knowledge that the waveforms in Fig. 5 were formed by a system imbalanced by additional SMF.

In practice, manufacturing DCF to cancel both second- and third-order dispersion to the tolerances demanded by subpicosecond pulses most often does not occur. The assumption of complete compensation of the cubic phase from the SMF by the DCF that allows Eq. (3) to be written is generally inaccurate. The ratio of $\beta_{2\mathrm{SMF}}$ to $\beta_{2\mathrm{DCF}}$ will vary slightly from the ratio of $\beta_{3\mathrm{SMF}}$ to $\beta_{3\mathrm{DCF}}$. Two DCFs with differing dispersion parameters can be used in concatenation to completely cancel both $\beta_{2\mathrm{SMF}}$ and $\beta_{3\mathrm{SMF}}$.[18] However, when the experimental system is designed with a single DCF type to exactly cancel second-order dispersion, the likely result is a small residual cubic phase term in Eq. (3) for all pulses in the output waveform. In the time domain each individual pulse comprising the larger waveform will take on an asymmetric shape. Because of the nature of the autocorrelation detection scheme, such pulse asymmetry is lost in the measured ACTs of Figs. 4 and 5. As discussed, an alternative experimental setup with a single DCF would achieve exact β_3 cancellation. The residual second-order dispersion could be removed with an additional dispersive element or be used to cancel the quadratic spectral phase originating from β_3 for a satellite pulse.

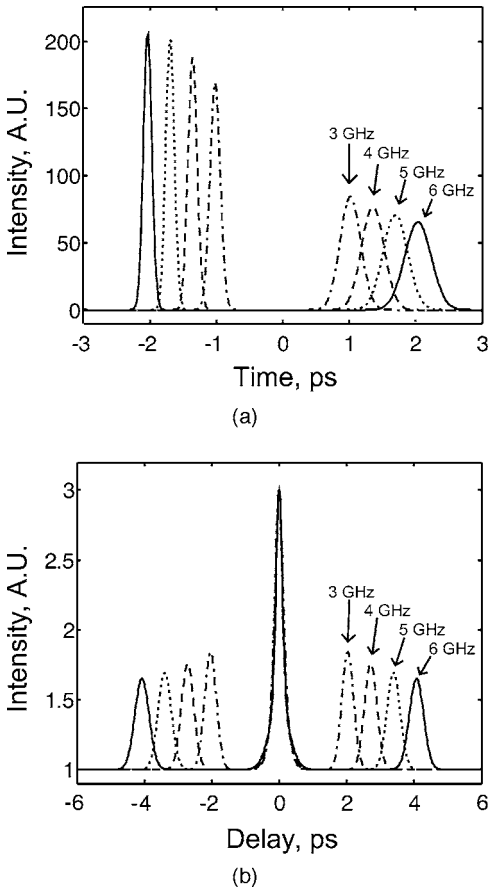

Fig. 6. Modeling results of pulse shaping in the combined presence of β_3 and residual second-order chromatic dispersion. (a) Intensity traces showing the asymmetric pulse pairs created for four modulation frequencies. For a system with 60 cm extra SMF (out of 2.6 km), the trailing pulses in the pairs are broadened significantly as compared with the lead pulses. (b) Intensity ACTs of the waveforms in part (a). The results in (b) show agreement with the experimental data displayed in Fig. 5.

5. CONCLUSION

We have demonstrated a novel approach to subpicosecond pulse shaping in a fiber-based arrangement. Spectral decomposition occurs in time by use of chromatic dispersion. Experimental results are presented and show strong agreement with the model developed. The ability to faithfully reproduce detected ACTs with simulations supports the validity of the linear system model. Examination of these results confirms the functionality of the dispersion-based pulse shaper while giving insight into the issues surrounding third-order chromatic dispersion as a distortion in the system. Making use of commercially available telecommunications fiber and instruments, the technique is highly suitable for integration with current communications systems. Confinement to a SMF removes the time–space interrelation inherent in traditional pulse-shaping devices, and it allows one to envision pulse shaping during propagation over long dispersion-compensated spans. The concept lends itself to new signaling methods including in-line schemes for coherent optical code-division multiple access. For signal processing applications requiring large TBWPs, higher-order dispersion is exposed as both a limitation to the temporal extent of generated waveforms and an advantage for creating asymmetric pulse shapes. Use of CFBGs as a fiber-integrated source of chromatic dispersion was theoretically presented as a method to create a distortion-free system. Ultimately, the CFBG method could realize the potential advantage of our dispersion-based technique over conventional time–space approaches used to achieve large

TBWPs. Dispersing the SDW to durations approaching a 100 ns time window and utilizing modulating devices in the tens of gigahertz range, more than 10^4 resolvable spots is conceivable with shaped waveforms lasting over a nanosecond. Alternative sources of modulation could be employed to replace the asymmetry in produced waveforms previously delivered by third-order chromatic dispersion. EO phase modulators and slower AO modulators offer single-sideband modulation resulting in satellite pulse generation on one side of the central point. The coupling of frequency and time shifts in the dispersion-based pulse-shaping system is a fundamental characteristic that must be factored in when large time shifts are needed and actual applications are considered.

APPENDIX A

In this appendix we describe the transmission characteristics of the EO modulator used to modulate the optical SDW field. Because of its Mach–Zehnder structure, the device retains a sinusoidal transmission characteristic versus applied voltage; however, because the optical field is of concern, the relationship described in Eq. (A1) has twice the period when compared with a traditional intensity modulation scheme, thus yielding

$$t_{\text{field}}(\nu) = \cos\left[\frac{\phi_0}{2} + \frac{\pi\nu(t)}{2V_\pi}\right]. \tag{A1}$$

Here ϕ_0 is the optical path-length difference of the two arms of the interferometer, $\nu(t)$ represents the signal voltage, and V_π is a voltage specification for the modulator. The signal voltage is in general $\nu(t) = V_b + V_m \sin(2\pi f_m t)$ where V_b is the bias voltage, V_m is the modulation amplitude, and f_m is the frequency of modulation. Inserting the signal voltage, Eq. (A1) expands to

$$t_{\text{field}}(V_b, V_m, f_m, t) = \cos\left(\frac{\phi_0}{2} + \frac{\pi V_b}{2V_\pi}\right)\cos\left[\frac{\pi V_m}{2V_\pi}\sin(2\pi f_m t)\right] - \sin\left(\frac{\phi_0}{2} + \frac{\pi V_b}{2V_\pi}\right)\sin\left[\frac{\pi V_m}{2V_\pi}\sin(2\pi f_m t)\right]. \tag{A2}$$

It is clear that the bias voltage plays an integral role in determining the comparative strength of the two terms. By appropriately selecting the bias voltage with knowledge of ϕ_0, the transmission of the field through the modulator will depend on a cosine of the applied signal voltage, a sine of the applied signal voltage, or a relative combination of each. To obtain a more meaningful view of this implication, a Fourier series expansion of the two terms gives

$$t_{\text{field}}(V_b, V_m, f_m, t) = \cos\left(\frac{\phi_0}{2} + \frac{\pi V_b}{2V_\pi}\right)\left[J_0\left(\frac{\pi V_m}{2V_\pi}\right) + \sum_{\substack{n=2 \\ n,\text{even}}}^{\infty} 2J_n\left(\frac{\pi V_m}{2V_\pi}\right)\sin(2\pi n f_m t)\right] - \sin\left(\frac{\phi_0}{2} + \frac{\pi V_b}{2V_\pi}\right) \times \left[\sum_{\substack{n=1 \\ n,\text{odd}}}^{\infty} 2J_n\left(\frac{\pi V_m}{2V_\pi}\right)\sin(2\pi n f_m t)\right]. \tag{A3}$$

Here $J_n(\,)$ represent an nth-order Bessel function of the first kind. Inspecting Eq. (A3) it is clear that the SDW is modulated by not only the applied signal voltage but also by a weighted collection of the entire set of harmonics. The bias voltage plays the role of selecting whether the odd harmonics, even harmonics (and dc), or both are represented in the modulation. The amplitude of the signal voltage, V_m, further determines the relative coefficient of each harmonic. Thus, for pulse-shaping applications, 2 degrees of freedom are present in controlling the outcome of the experiment when such a Mach–Zehnder device is employed. Following the descriptions given by Eqs. (4) and (5), the bias and signal amplitude are used to control the relative strength of the coefficients A and B. Although null biased, the modulator that is experimentally used offers an extinction ratio of $\sim$19 dB for a 15 dBm driving voltage. This level of carrier suppression justifies our setting the A coefficient to zero when desired, and demonstrates the ability to extinguish the even harmonics. Ultimately, because the spectral components of the modulating signal manifest themselves as pulses at the output of the pulse shaper, controlling the bias and amplitude allows for creation of a pulse sequence of varying heights and spacing with application of a single microwave tone. Limitation to the height of a satellite pulse comes from the Bessel function expansion, which necessitates the creation of higher harmonics at large driving voltages. Figure 2 of Ref. 9 shows clear signs of higher harmonics in the detected ACT stemming from a 23 dBm driving voltage. As an important experimental note, appropriate selection of the electronic signal parameters allows one to work around the frequency limitations of the modulator or signal generator to achieve larger pulse separations without adding more matched fiber [i.e., increasing z in Eq. (4)].

ACKNOWLEDGMENTS

This research was supported by the Defense Advanced Research Projects Agency, the Applied Micro Circuits Corporation, the U.C. Discovery Grants Program, the National Science Foundation, and the U.S. Air Force Office of Scientific Research. Dmitriy Panasenko gratefully acknowledges the support of the Fannie and John Hertz Foundation.

The e-mail address for Robert Saperstein is res@emerald.ucsd.edu.

Dmitriy Panasenko is now at the Optical Sciences Center, Tucson, Arizona 85721.

REFERENCES

1. W. S. Warren, H. Rabitz, and M. Dahleh, "Coherent control of quantum dynamics: the dream is alive," Science **259**, 1581–1589 (1993).
2. J. A. Salehi, A. M. Weiner, and J. P. Heritage, "Coherent ultrashort light pulse code-division multiple-access communication systems," J. Lightwave Technol. **8**, 478–491 (1990).
3. A. M. Weiner, D. E. Leaird, J. S. Patel, and J. R. Wullert II, "Programmable shaping of femtosecond optical pulses by use of 128-element liquid crystal phase modulator," IEEE J. Quantum Electron. **28**, 908–920 (1992).
4. M. A. Dugan, J. X. Tull, and W. S. Warren, "High-resolution acousto-optic shaping of unamplified and amplified femtosecond laser pulses," J. Opt. Soc. Am. B **14**, 2348–2358 (1997).
5. A. M. Weiner, J. P. Heritage, and E. M. Kirschner, "High-resolution femtosecond pulse shaping," J. Opt. Soc. Am. B **5**, 1563–1572 (1988).
6. T. Kurokawa, H. Tsuda, K. Okamoto, K. Naganuma, H. Takenouchi, Y. Inoue, and M. Ishii, "Time-space-conversion optical signal processing using arrayed-waveguide grating," Electron. Lett. **33**, 1890–1891 (1997).
7. M. M. Wefers and K. A. Nelson, "Space-time profiles of shaped ultrafast optical waveforms," IEEE J. Quantum Electron. **32**, 161–172 (1996).
8. D. E. Leaird, A. M. Weiner, S. Kamei, M. Ishii, A. Sugita, and K. Okamoto, "Generation of flat-topped 500-GHz pulse bursts using loss engineered arrayed waveguide gratings," IEEE Photon. Technol. Lett. **14**, 816–818 (2002).
9. R. E. Saperstein, D. Panasenko, and Y. Fainman, "Demonstration of a microwave spectrum analyzer based on time-domain optical processing in fiber," Opt. Lett. **29**, 501–503 (2004).
10. B. H. Kolner, "Space-time duality and the theory of temporal imaging," IEEE J. Quantum Electron. **30**, 1951–1963 (1994).
11. Y. C. Tong, L. Y. Chan, and H. K. Tsang, "Fiber dispersion or pulse spectrum measurement using a sampling oscilloscope," Electron. Lett. **33**, 983–985 (1997).
12. S. Longhi, M. Marano, P. Laporta, O. Svelto, and M. Belmonte, "Propagation, manipulation, and control of picosecond optical pulses at 1.5 m in fiber Bragg gratings," J. Opt. Soc. Am. B **19**, 2742–2757 (2002).
13. J. Azaña and L. R. Chen, "Synthesis of temporal optical waveforms by fiber Bragg gratings: a new approach based on space-to-frequency-to-time mapping," J. Opt. Soc. Am. B **19**, 2758–2769 (2002).
14. P. C. Chou, H. A. Haus, and J. F. Brennan III, "Reconfigurable time-domain spectral shaping of an optical pulse stretched by a fiber Bragg grating," Opt. Lett. **25**, 524–526 (2000).
15. S. Shen, C. C. Chang, H. P. Sardesai, V. Binjrajka, and A. M. Weiner, "Effects of self-phase modulation on sub-500 fs pulse transmission over dispersion compensated fiber links," J. Lightwave Technol. **17**, 452–461 (1999).
16. G. P. Agrawal, *Nonlinear Fiber Optics*, 3rd ed. (Academic, 2001).
17. M. Durkin, M. Ibsen, M. J. Cole, and R. I. Laming, "1 m long continuously-written fiber Bragg grating for combined second- and third-order dispersion compensation," Electron. Lett. **33**, 1891–1893 (1997).
18. L. F. Mollenauer, P. V. Mamyshev, J. Gripp, M. J. Neubelt, N. Mamysheva, L. Grüner-Nielsen, and T. Veng, "Demonstration of massive wavelength-division multiplexing over transoceanic distances by use of dispersion-managed solitons," Opt. Lett. **25**, 704–706 (2000).